RSC Advances

PAPER

View Article Online
View Journal | View Issue

Cite this: *RSC Adv.*, 2017, **7**, 44356

White light and multicolor emission tuning in Ag nanocluster doped fluorophosphate glasses

Hssen Fares,* Tarcio Castro, Juliane Resges Orives, Douglas Faza Franco and Marcelo Nalin

Received 8th August 2017
Accepted 11th September 2017

DOI: 10.1039/c7ra08778k

rsc.li/rsc-advances

The emission properties of Ag nanoclusters (Ag NCs) dispersed in a transparent fluorophosphate glass host have been studied. The as-prepared glass shows that the Ag NCs emit a broad white emission band almost covering the entire visible region. By changing the excitation wavelength it is possible to tune the emission from blue to yellow. The spectral width of the white light is most likely due to the presence of a variety of Ag NCs with different sizes, particularly emitting in the blue, green and red regions. The possible interaction mechanism between the different Ag species was also elucidated. The observed results provide a new platform to acquire a broad band tunable light source.

I. Introduction

The luminescence of silver by quantum confinement has attracted interest owing to a variety of potential novel applications, such as biomedical applications, nano-sensors, white light generation, luminescent lamps, flexible monitors and down-shifting of the solar spectrum for enhanced efficiency in solar cells.[1–10] In general, the optical responses of metals depend on their sizes. In the case of metallic nanoparticles (NPs), the luminescent properties are very poor but they absorb light strongly due to surface plasmon resonance effects arising from the collective oscillation of conduction electrons upon interaction with light.[11–13] However, the reduction of the particle size down to a few nanometers, approaching the Fermi wavelength, leads to a breakup of the continuous band structure of the metal into discrete energy levels.[11] In this case, the metal is called a NC in which the collective oscillation of electrons is obstructed, otherwise the particle is not plasmonic.[11] In contrast, interaction with light is still possible though, *via* electronic transitions between the energy levels and thus NCs are capable of intense light absorption as well as for tunable visible emission both in the linear and non-linear optical regime.[11,14]

Recently, special attention is paid to oxide glassy materials doped with luminescent Ag NCs owing their superior mechanical, structural and optical properties which may give more benefits for photonic applications.[15,16] In fact, oxide glass host materials are exceptionally attractive due to their high metal solubility,[17] which allows tuning the material optical properties based on the dopants concentration. Most recently, a great progress has been achieved by Tikhomirov *et al.* that demonstrated that the introduction of CdF_2/PbF_2 into silicate glass network favors the dispersion of Ag NCs across the whole bulk glass.[18–20] It was also demonstrated that the emission of Ag NCs depends to the size and can be tuned from UV, throughout VIS, to near-IR by selection of the proper excitation wavelength. However, the luminescent properties of the Ag NCs depend not only on their size but also on the choice of the host material.[15] Since the average size distribution decreases in the medium with high viscosity due to slow diffusion of silver atoms towards nuclei,[21] oxyfluoride glasses based on silica, which present a very low viscosity, diminished their potential in photonic applications based in the size distribution of small NCs. Particular properties of fluorophosphate glass such as high viscosity, low glass transition temperature, low melting point, and low optical dispersion, allow this host matrix to be an advantageous over oxyfluoride glass based silica.[22,23]

In this direction, Ag doped fluorophosphate glasses were prepared by simple single-step melt-quenching route. To the best of our knowledge, rare earth free white light was generated from Ag NCs dispersed in fluorophosphates glass.

II. Experimental details

The Ag NCs doped fluorophosphate glasses were prepared by conventional melt-quenching method using high-purity compounds (99.9%, Sigma-Aldrich). The chemical formula of the glass host, $50NaPO_3$– $25ZnF_2$–$15CdF_2$–$10YF_3$ mol%, was adjusted to ensure its glass stability against devitrification. $AgNO_3$ (purity 99.9%) was added, in different mol%, ($x = 0$, 3, 5, 7 and 10 mol%, labeled as Ag0, Ag3, Ag5, Ag7 and Ag10, respectively) as a resource of silver NCs. Approximately 7 g batches were mixed and then melted in an alumina crucible at 900 °C for 1 h under ambient atmosphere. The melt was casted into a pre-heated stainless steel mold at 320 °C (value obtained

Institute of Chemistry, São Paulo State University, UNESP, P. O. Box 355, Araraquara, SP, 14800-060, Brazil. E-mail: fares.hssen@gmail.com

from DSC measurements) to remove any residual internal stress induced by the rapid cooling of the glass melt. The glass was left at such temperature during 1 h before to be cooled down to room temperature. Finally, the obtained glasses were cut and polished with thickness of 2 mm for optical measurements.

Transmission electron microscopy (TEM) investigations were carried out using a Philips CM200 equipment operating at 200 kV and equipped with X-ray energy dispersive spectroscopy (EDS) Bruker model XFlash 6TI30. Samples were put in an agate mortar and grinded thoroughly. Then, ~0.1 mg of powder and 10 mL of isopropyl alcohol were placed in a glass vial that was placed in an ultrasonic bath for 15 min to disperse the nano-powder. Some drops of this suspension were applied on a copper grid coated with carbon film. Afterward, the deposited sample on the copper grid was dried in air before TEM analysis.

UV-vis absorption spectra as well as transmission spectra were recorded using a Varian Cary 500 double beam spectrophotometer on the polished samples of 2 mm thickness. Excitation and emission spectra were obtained using Fluorolog (Horiba Jobin Yvon) equipment. Both measurements were obtained from glass pieces. For excitation measurements the emission wavelength was set at 550 nm. Slits were adjusted to lead a resolution of 1 nm for both excitation and emission. All measurements were performed at room temperature and corrected by the instrument response.

III. Results and discussion

III.1. Optical properties and nanostructure analysis

Fig. 1(a) shows the pictures of prepared fluorophosphate glasses under daylight and UV light for 254 and 365 nm excitation wavelengths, Fig. 1(b) and (c), respectively. As we can see from Fig. 1(a), the Ag doped fluorophosphate glasses are homogeneous, completely transparent and are colorless for samples containing low Ag content and pass to yellow color for samples containing higher concentration of $AgNO_3$. The change in color is induced by the formation of Ag NCs and/or Ag NPs within the glass network with large amounts of $AgNO_3$ and will be discussed below. Under excitation with UV lamp at 254 nm (Fig. 1(b)), a strong blue emission has been detected, which increases with the Ag doping level (samples Ag3 and Ag5), and becomes green in the glasses with higher concentration of silver (samples Ag7 and Ag10). On the other hand, luminescence image of the same glass samples, excited with a UV lamp at 365 nm indicates a different color rendering of the emission from white (Ag3 and Ag5 glass samples) to yellow (Ag7 and Ag 10 glass samples) according to their $AgNO_3$ content, as depicted in the Fig. 1(c). Such behavior point out that the emission of Ag particles doped fluorophosphate glasses depend strongly on the excitation wavelength and structure of the Ag particles dispersed into the glass network.

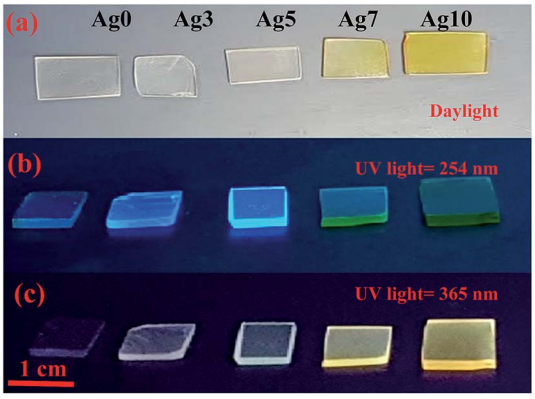

Fig. 1 Daylight pictures (a), luminescence images excited by a UV lamp at 254 nm (b) and 365 nm (c) for all prepared glasses.

The transmission spectra from ultraviolet to near-infrared range of the prepared glasses are presented in Fig. 2(a). As observed, the transparency of Ag*x* glass samples is altered with increasing of Ag doping level. Firstly, the ultraviolet cut-off wavelength is red-shifted from 280 to 345 nm and it is also accompanied by a curvature of the top of transmission edge. Secondly, the maximum transmission in near-infrared range slightly decreases from 87% to 82% with increasing of $AgNO_3$ concentration. The evolution of transmission under different doping condition can also be evident from the pictures in Fig. 2(a). Both effects can be explained by the presence of scattering centers within the glass network, whose concentration, dimensions and/or shape evolve with increasing $AgNO_3$ concentration. This observation is strongly proved from the absorption spectra of the corresponding glasses presented in Fig. 2(b). In fact, a weak absorption peak located at about 415 nm is detected in the Ag7 glass sample with a full width at half maximum of ~50 nm, which is typically attributes to the presence of SPR of Ag NCs.[24,25] In addition, the plasmon absorption band becomes more intense with increasing of $AgNO_3$ concentration. These effects are related to an increase of size of the Ag NCs and/or in the amount of Ag NPs within the glass network. For samples with low (3 mol%) and intermediate (5 mol%) $AgNO_3$ doping, it can be clearly seen that the absorbance spectra do not show any absorption bands in the violet/UV part of the spectra. Similar absorption features were observed in other previous works, where the authors assigned this behavior to the reduced particle size, which is too small (1–2 nm) to generate a SPR absorption band.[26–28]

The nanostructure properties of the prepared fluorophosphate glasses were analyzed by means of transmission electron microscopy (TEM) and selected area electron diffraction pattern (SAED). TEM, SAED analysis and diameter distribution of prepared samples were carried out for two different concentrations of $AgNO_3$ (5 and 10 mol%). The size distributions of the silver NCs of the samples were obtained by the analysis of ~250 particles. Fig. 3 shows the TEM micrographs of Ag5 (Fig. 3(a) and (c)) and Ag10 (Fig. 3(b) and (d)) glass samples. The micrographs for Ag doped fluorophosphate glasses shows that spherical particles, visible as dark contrast spots, are evenly dispersed in the glassy matrix with average diameter (AD) of 2.58 and 3.29 nm for Ag5 and Ag10 glass samples, respectively (see histogram in Fig. 3(e and f)). One can see that the Ag particles remain amorphous in the prepared glass samples. In fact, the amorphous character of Ag clusters is evidenced by SAED pattern (Fig. 3(g and h)), which contains only diffuse diffraction rings typical for an amorphous phase.

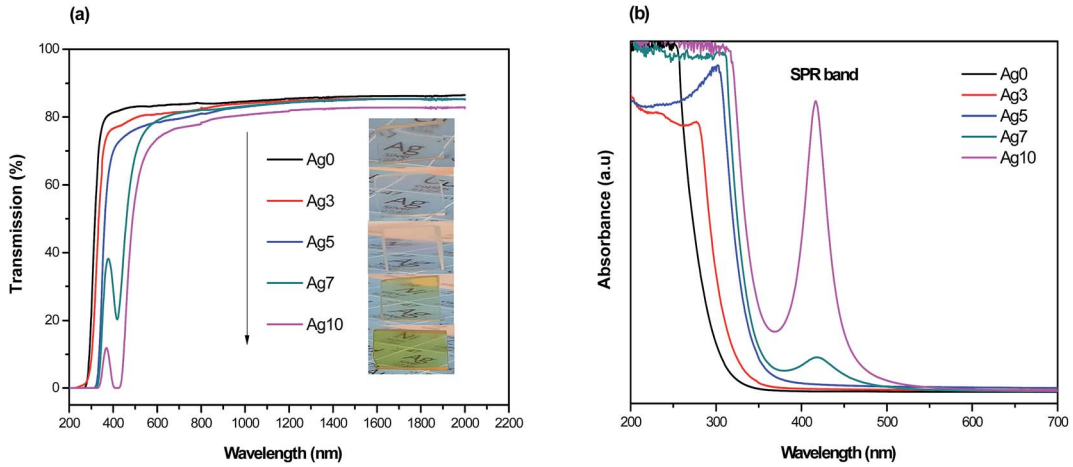

Fig. 2 (a) UV-visible and near infrared transmission spectra of glass samples as a function of $AgNO_3$ concentration with their corresponding photograph presented in inset. (b) Absorption spectra of Ag NCs doped prepared glasses.

It should be noted that these tiny particles are spontaneously formed and without any heat treatment. In this sense, a reduction mechanism must be considered which is responsible for the particle formation of the tiny Ag particles during melting. Perhaps the silver reduction could occur due to the electrons extracted directly from defects that are intrinsic to the glass, namely F^- vacancies residing within fluorophosphate glasses. In fact, the mechanisms for the formation of Ag NCs within oxyfluoride glass host have been suggested recently. According to Tikhomirov *et al.*[3] the F^-centers residing in glass network, where an electron substitutes onto the place of an F^-, favors the formation, stabilization and homogeneous dispersion of Ag NCs. In such condition, the electrons released diffuse to occupy the vacant sites such as Ag^+ ions. The reduction mechanism resulting in the formation of Ag NCs is described through the following reactions of eqn (1) where a neutral Ag NCs and Ag^+ ions intrinsically condense and resulting the formation of other Ag NCs, consisting of a few Ag atoms defined as Ag_m^{x+} clusters, such as Ag dimers (Ag_2^+), Ag trimers (Ag_3^{2+}) and tetramers (Ag_4^{2+}).[29]

$$\begin{aligned} Ag^+ + 1e^- &= Ag^0 \\ Ag^+ + Ag^0 &= Ag_2^+ \\ Ag^0 + Ag_2^+ &= Ag_3^+ \\ Ag^+ + Ag_2^+ &= Ag_3^{2+} \\ Ag^0 + Ag_3^{2+} &= Ag_4^{2+} \end{aligned} \quad (1)$$

It should be noted here that the average diameter of the large particles appears to be around 5 (±1) nm. Note that a heat treatment was carried out at 320 °C, which is below the glass transition temperature (385 °C), to remove any residual internal stress induced by the rapid cooling of the glass melt. Thus, the larger particles observed in TEM micrographs (>5 nm) are most likely generated during the sample preparation. In fact, the Ag particles within fluoride network present very high mobility already at 300 °C.[3] Thus, the large Ag particles observed are formed during the annealing process due to the high mobility of the Ag particles in the fluorophosphate matrix.

III.2. Excitation and emission spectra dependences on Ag nanoclusters concentrations

The excitation spectra for prepared samples were recorded at several wavelengths in the range of 250–550 nm. Results obtained at 550 nm are reported in Fig. 4 and 5. One can see that excitation of Ag NCs doped fluorophosphate glasses depend strongly to silver concentration, and the local environment around the Ag particles. In fact, for samples with low Ag doping (Ag3), the excitation spectrum is fitted by a single Gaussian band peaked at 278 nm, whereas the excitation spectra for intermediate Ag doping (Ag5 and Ag7) are fitted by two Gaussian bands centered at 278 and 360 nm while at higher Ag doping (Ag10) the spectrum is fitted by three Gaussian bands, centered at 278, 365 and 458 nm, respectively (Fig. 5(a, b, c and d)). The two excitation bands spanning the range from 270 to 400 nm are related to different types of Ag NCs with different size while the band centered at 458 nm for the Ag10 glass samples can be ascribed to the presence of a new emitting center, presumably silver particles with large average diameter. A similar broad excitation at around 270 nm which is related to Ag NCs, more precisely Ag_4^{2+} NCs, was also reported for other matrixes.[30,31] As visible in the figure, the curve fits are quite satisfactory; however, the uncertainty in the location of the second and the third bands maximum beyond the experimentally observed wavelength range is not crucial for the following data analysis.

Obviously, a difference in the relative intensity of the two bands is observed (centered at 270 and 360 nm) with the increases of $AgNO_3$ concentration. The band at higher wavelength (360 nm) being more prominent in Ag10 glass samples and shifts to longer wavelength with increases of the $AgNO_3$ concentration. These unique concentration-dependent PLE properties could not be related to glass defect centers, but are strongly pointed to the multiplicity of size/site distribution of Ag NCs as a consequence of the perturbation induced by the rearrangement of the Ag species.[32]

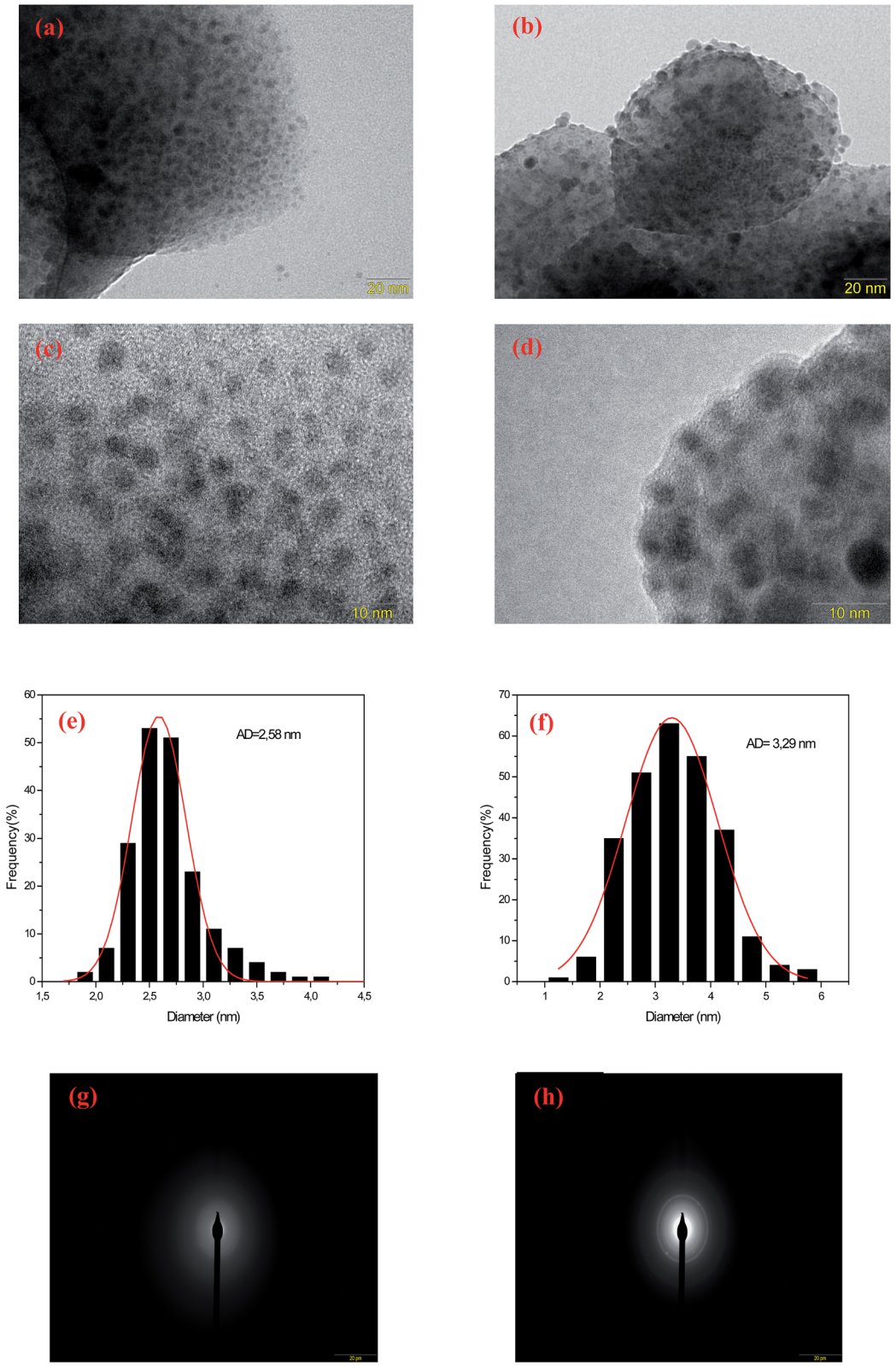

Fig. 3 TEM images of Ag5 (a and c) and Ag10 (b and d) glass samples as well as corresponding diameter distribution (e) and (f), respectively. Selected area electron diffraction pattern (SAED) taken from Ag5 (g) and Ag10 (h) glass samples.

The normalized emission spectra of the Ag*x* glass samples upon excitation of 360 nm are shown in Fig. 6(a). It is seen in Fig. 6(a) that the Ag NCs emit a broad luminescence band almost covering the visible light region (from 400 to 800 nm). Note that the un-doped glass sample (Ag0) did not show any appreciable emission. Therefore, the luminescence in the

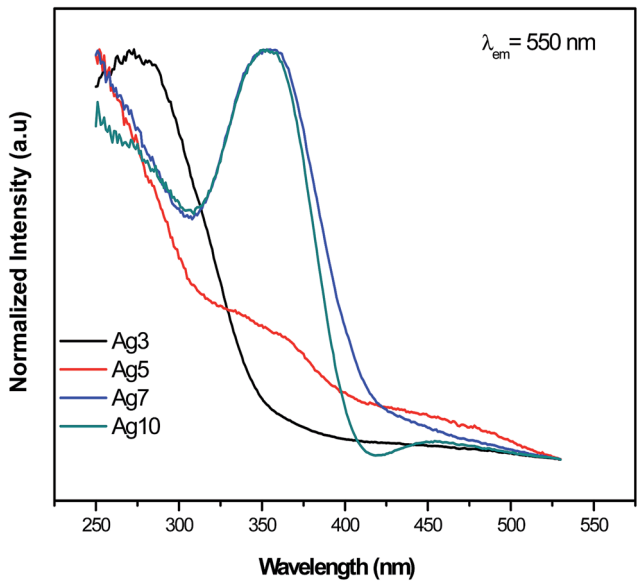

Fig. 4 Normalized excitation spectra (PLE). The emission was fixed at 550 nm.

prepared glasses is due to Ag particles. A perfect concentration dependent luminescent performance is observed. In fact, increasing the Ag doping level, the emission spectra are shifted to the red at the same excitation wavelength indicating that the average Ag NCs size does increases with the Ag doping. The histograms of the prepared glasses support this point of view (Fig. 3(e and f)). Additionally, the CIE chromaticity diagram for the prepared glasses reported in Fig. 6(b) indicates a different color rendering of the emission from blue (Ag3) to yellow (Ag7 and Ag 10 glass samples) while Ag5 glass sample indicates a white emission as shown in the corresponding photograph in Fig. 1. These results point out an unhomogeneous broadening due to a number of factors, including number of Ag atoms comprising the NCs, different surroundings in the fluorophosphate network, shape and size/site distribution.

On closer inspection, the spectra with superimposed broad bands were de-convoluted using a Gaussian distribution as shown in Fig. 6(c). All the emission spectra were fitted to three Gaussians bands peaked at about 420, 535 and 620 nm. These bands can be ascribed to the presence of different types of luminescence centers which will be called further, for simplicity and as proposed in previous work,[33] as the blue, green and red Ag NCs. In fact, these luminescent Ag NCs have been argued to be mostly the Ag_m^{x+} species with different sizes. A similar result reported that the broad luminescence band is commonly ascribed to small Ag NCs.[29]

An analysis of these spectra highlights on the mechanism governing the emission of Ag NCs within prepared fluorophosphate glasses. One can see that the green and the red bands become more prominent with increasing Ag concentration at the expense of the blue band which decreases with the

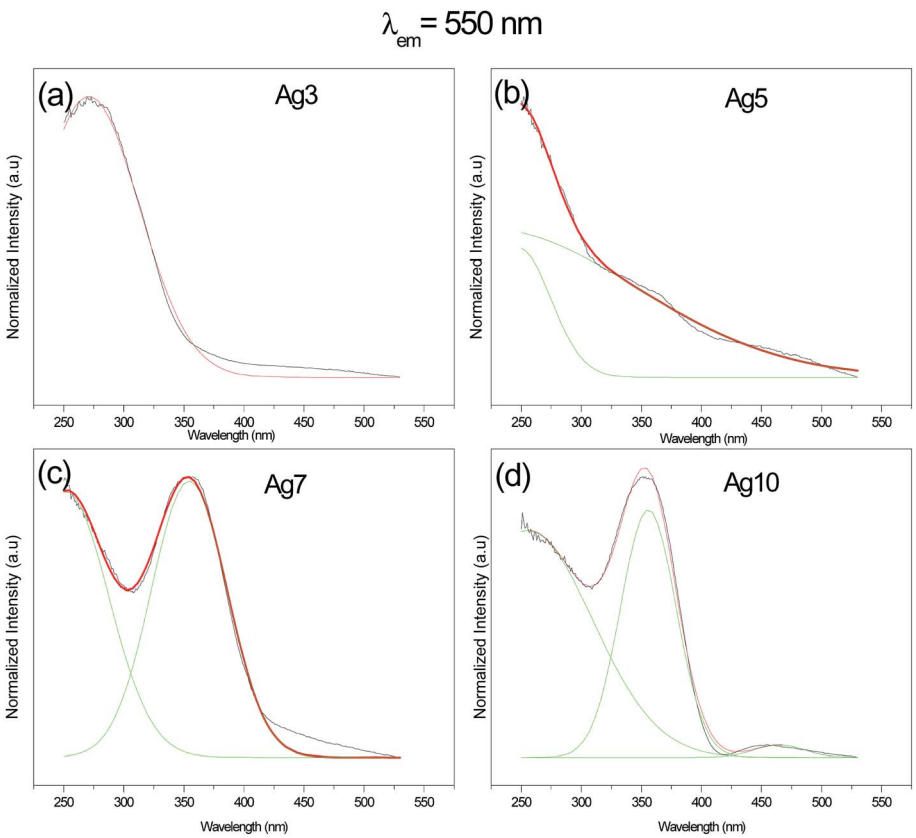

Fig. 5 The de-convoluted excitation spectra of Ag NCs doped fluorophosphate glasses.

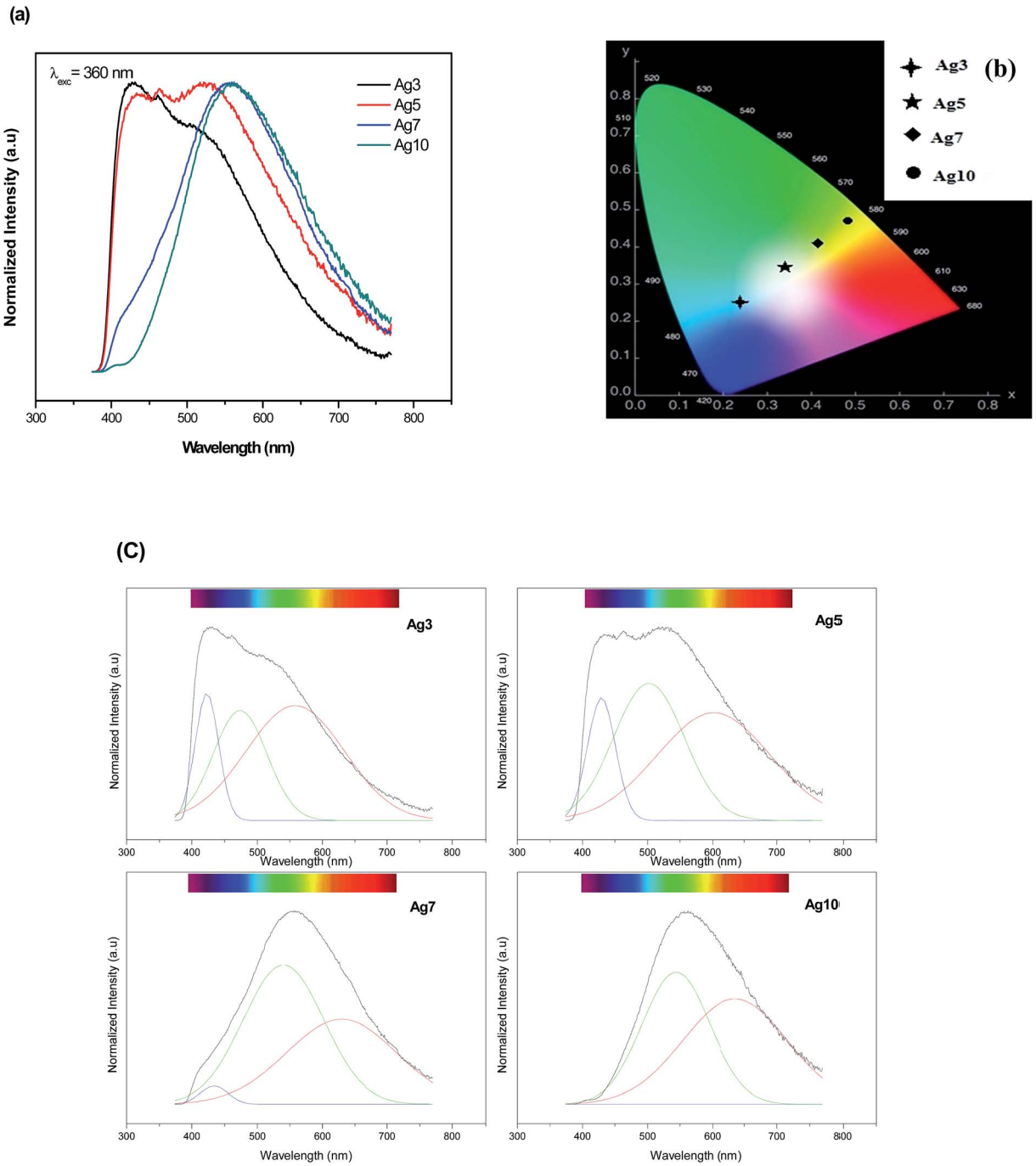

Fig. 6 Normalized emission spectra (a) and the CIE chromaticity diagram (b) of prepared samples upon 360 nm excitation. (c) The deconvoluted emission spectra of Ag NCs doped fluorophosphate glasses.

increases of Ag doping level, this effect being stronger in Ag10 glass sample. Two mechanisms can explain this effect: variations size/site distribution of Ag NCs and/or an energy transfer occurs between Ag NCs close to each other.

It was previously demonstrated that the radiative transitions originated from outer d-orbitals which means that the luminescence is sensitive to local crystal fields.[15] As the silver concentration increases, the number of silver atoms in NCs rises up and then increasing the size of the NCs. Consequently, the crystal field environment of Ag NCs is affected which leads to the change in the intensity as well as the shape of the emission band. According to Tikhomirov *et al.*[3] the short wavelength part of the Ag emission spectra corresponds to the emission by smaller size Ag NCs (called "blue" NCs), while the long wavelength part corresponds to emission by larger size NCs (called "green" and "red" Ag NCs). Hence, the decreases in the blue emission as the silver concentration increases can be explained by the decrease of the amount of smaller size Ag NCs.

On the other hand, the increases of green and red emissions are related mostly to the evolution of the amount of larger NCs called here "red" and "green" Ag NCs. As described before, the evolution of the different silver species with the increase in the $AgNO_3$ concentration can be described by a two-step mechanism. The first step consists in the formation of color centers (Ag^0 and Ag^{2+}).[29] Then, when the concentration of silver is high enough, the amount of color centers is sufficient to allow their clustering in Ag_m^{x+} species. As the concentration of silver increases, the reduction rate also increases and results in the enlargement of size and concentration of Ag NCs. This is maybe explaining the increases of "green"/"red" NCs at the expense of the "blue" NCs. Our TEM images support this point of view since the volume fraction of large NCs (>3 nm) increases while the volume fraction of small NCs (<2 nm) decreases with the increases of Ag doping level.

Additionally, Fig. 7(a and b) depicts the normalized excitation and emission spectra respectively of the fluorophosphate glass doped with 7 mol% $AgNO_3$ monitored/excited at different wavelengths. As we can see, a shift of the detection and excitation wavelength from blue to the red results in red shift of the respective excitation and emission spectra in addition to the evolution in the relative intensity of the broad band related to Ag NCs spanning the range from 270 to 400 nm. A similar behavior has been detected in previous work and as explained by M. V. Shestakov *et al.*[34] this unique wavelength-dependent emission and excitation properties is related to the dispersion of Ag NCs with varying surroundings, *i.e.* with varying an Ag NCs site, and also to the presence of a variety of Ag NCs with different sizes.

The second possible factor responsible for this effect is the energy transfer between neighboring Ag NCs. Recently, a model has been achieved by A. S. Kuznetsov *et al.* in which they demonstrate that energy transfer occurs from the smaller Ag NCs emitting in the blue to either more larger Ag NCs emitting in the green and further in the red, or directly to Ag NCs emitting in the red.[19]

Combining the TEM results and emission spectra of prepared fluorophosphate glasses, we can conclude that, when the size of "blue" Ag NCs reaches a critical value, they apparently cease to emit and/or they transfer energy to "green" and "red" NCs. Hence, the luminescence properties of Ag NCs are mostly defined by size as well as by the number of Ag NCs within glass network. The relationship between an Ag NCs size and its fluorescence proprieties will be discussed more in the next section.

III.3. Emission spectra dependence on excitation wavelengths

It is important to evaluate the excitation dependence on the emission properties of Ag NCs doped glasses for practical applications. Since a white color emission is generated from Ag5 glass sample with excitation wavelength near to 360 nm, we turn our attention into improving this result which maybe provides useful information for applications in the fields of white LEDs. Previously, the excitation spectrum of Ag5 glass sample indicates that the most intense excitation wavelengths for Ag NCs were located at 270 and 360 nm, respectively. In the following section, these wavelengths were used as optimal excitation wavelengths to record emission spectra of Ag5 glass sample.

The normalized emission spectra of the Ag5 sample upon excitation of different wavelengths according to the absorption band in the range of 270–360 nm are shown in Fig. 8(a). As we can see, the position and shape of the emission depend strongly on the excitation wavelength. When the excitation wavelength is shorter than 310 nm, the emission spectra merely exhibits a single band with the maximum shifting from the violet to the blue region, *i.e.*, from 420 to 470 nm. On the other hand, dual mode emission bands in the range of 400–620 nm covering blue

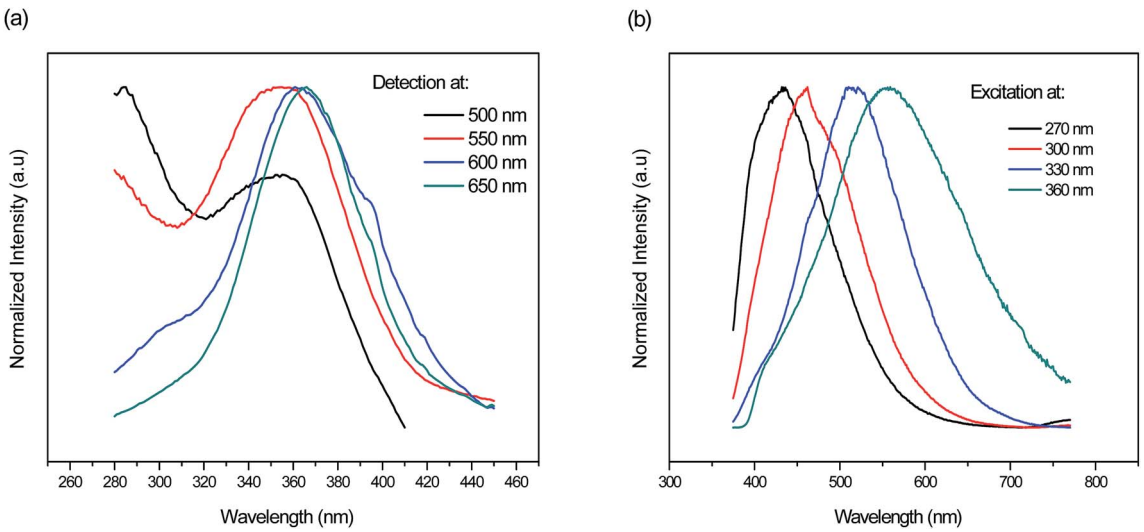

Fig. 7 Normalized (a) excitation and (b) emission spectra of the fluorophosphate glass doped with 7 mol% $AgNO_3$ monitored/excited at different wavelengths respectively.

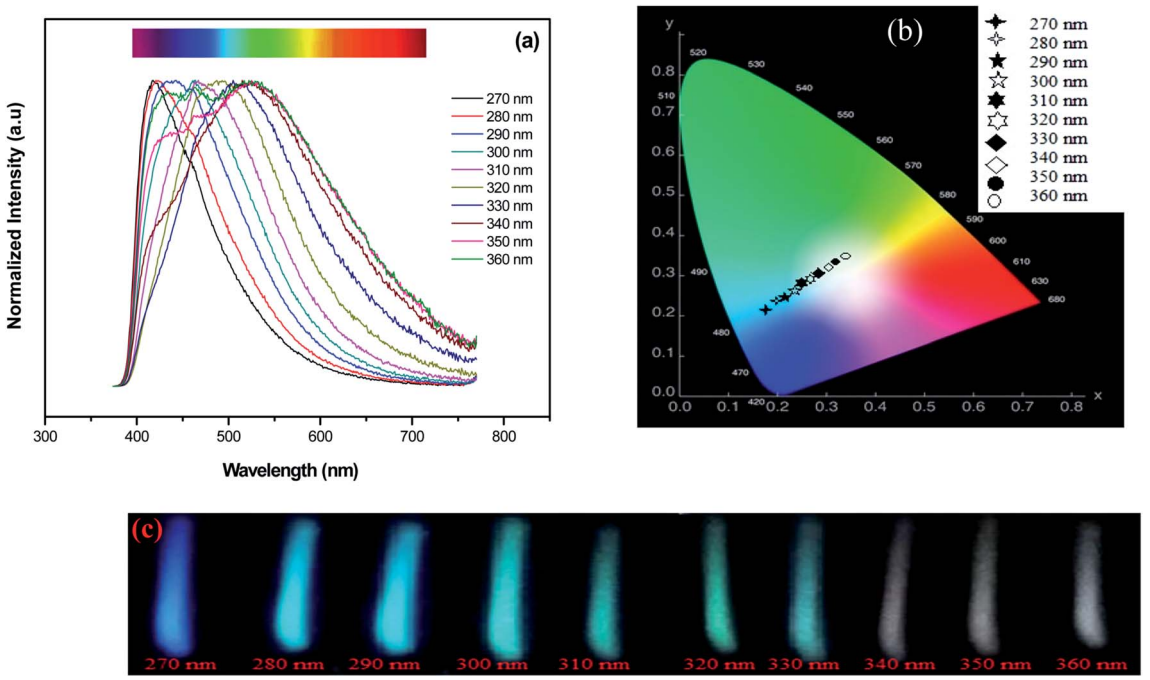

Fig. 8 Normalized emission spectra (a) the CIE chromaticity diagram (b) and (c) luminescence images showing multicolor emission of 5 mol% $AgNO_3$ doped sample excited/monitored at different wavelengths.

and green region gradually emerge with excitation wavelength in the range of 310–330 nm. Excitation at longer wavelength (<340 nm) resulting in a broad luminescence band almost covering the visible light region (from 400 to 800 nm). In fact, there is a strong relationship between an Ag NCs size and its fluorescence excitation wavelengths[35] As we can see, the emission maximum was found to shift to longer wavelengths with increasing excitation wavelengths from 270 nm to 360 nm, which confirms a distribution of Ag NCs with different size and this match well with the earlier reported respective spectra of Ag NCs doped oxyfluoride glasses.[24,29] A similar shifting with excitation wavelength has been detected in semiconductor quantum dots, and it has been related to the size-selective excitation of the quantum dots,[15,36] in other words, the emission properties depend on the Ag NCs size. Thus, this unique wavelength-dependent emission and excitation properties are strongly related to Ag NCs comprising different numbers of Ag atoms, otherwise, related to the presence of a variety of Ag NCs with different sizes and geometry, particularly emitting in the blue, green and red region.[3,33]

As described before on previous works[3] the blue part of the Ag emission spectrum corresponds to the emission by smaller size Ag NCs (called in ref. 33 as "blue" NCs), while the green and red parts correspond to emission by larger size NCs (called in ref. 33 as "green" and "red" NCs). The chromaticity diagram presented in Fig. 8(b) resumes the color rendering tuning obtained from the glass samples for different excitation wavelengths. As it is seen from Fig. 8(c), white color emission with varying tint can be generated under UV excitation (>330 nm). The obtained emission results suggest that sample Ag5 is useful for white light generation in fluorescent lamps and UV LEDs.

To obtain a deeper insight about the mechanism governing the emission of Ag NCs, the microsecond decay curves of Ag5 glass sample at different wavelengths upon 360 nm excitation were recorded. The emission was detected at 420, 550 and 620 nm; the results are presented in Fig. 9. The decay curves are fitted by a double exponential function given by:[31]

$$I(t) = A_1 \exp\left(\frac{-t}{\tau_{\text{fast}}}\right) + A_2 \exp\left(\frac{-t}{\tau_{\text{slow}}}\right) \quad (2)$$

where I is the luminescent intensity, A_1 and A_2 constants, t the time, τ_{fast} and τ_{slow} the fast and long lifetimes, respectively. The calculated lifetimes, as shown in Table 1, indicates that the luminescent dynamics of Ag NCs dispersed in glass host are in the microsecond regime. The fast and slow regimes evident in the lifetime data. In addition, the results show that the lifetimes are shorter for blue emission wavelengths relative to the green and red emission wavelengths. We believe that the multiplicity of size/site distribution of Ag NCs could be responsible for the obtained lifetimes. The obtained experimental curves are consistent with those reported for emitting Ag NCs dispersed in other glasses.[19,31]

As we can see, the slow PL lifetimes of the multi-exponential decay are shorter at blue emission (68 μs) wavelengths than for green and red emissions (114 and 131 μs, respectively). Analogous lifetime dependence was observed for the luminescence decay of Ag NCs doped Y-zeolites[37] interpreted using a model involving four-level system: two singlet states and two close thermalized metastable triplet levels. The short lifetime (68 μs) is due to the allowed singlet–singlet transition while the longer lifetimes (114 and 131 μs) are due to the forbidden triplet–singlet transition, as it was explain in previous works.[38]

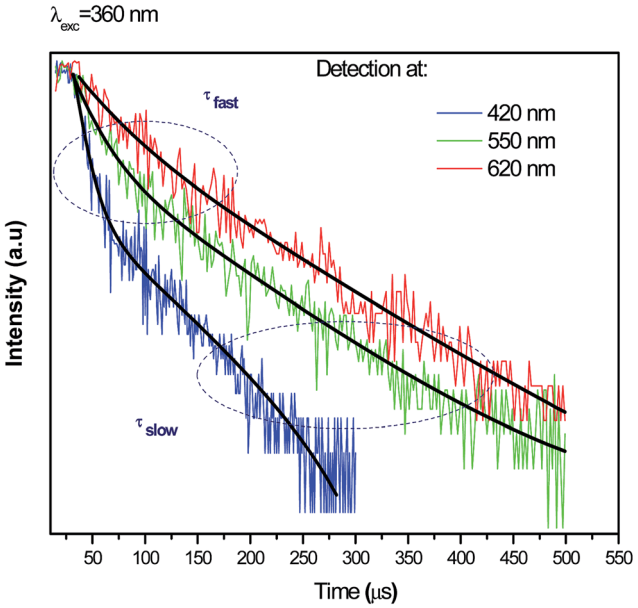

Fig. 9 Luminescence decay curves for different detected wavelengths upon excitation at 360 nm.

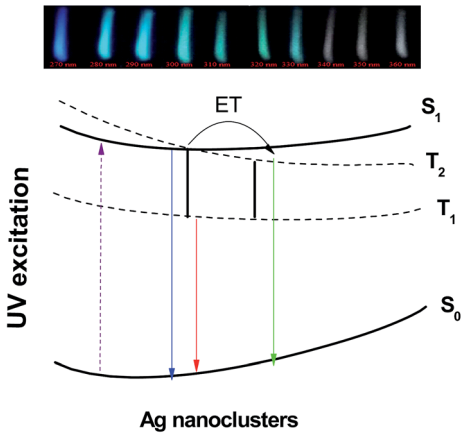

Fig. 10 Schematic configuration coordinate diagram of Ag_m^{x+} NCs is referenced to the paper by Velázquez *et al.*[19]

Moreover, Hang Lin *et al.*[31] explain the observed distinct lifetimes to the multiplicity of size/site distribution of Ag NCs.

It is far beyond the scope of this contribution to perform a computational methods of quantum chemistry for a more comprehensive mechanism governing the luminescence of Ag NCs, as well as, the reduction mechanism of Ag NCs within the new glass system, however, the results reported herein are still interesting and some general considerations can be drawn from the experimental results, particularly TEM microscopy, luminescence decay curves and the obtained excitation and emission spectra of prepared glasses. Combining all, we can conclude that, emission of blue NCs occurs by fast singlet–singlet transition while the green and red NCs occur by slow triplet–singlet.

The simplified energy level diagram suggested in Fig. 10 illustrates the excitation and emission mechanism in Ag_m^{x+} NCs resulting the white light. We follow here the notations proposed by J. J. Velázquez *et al.*[19] According to the authors, only the lowest electronic states contribute on the process of luminescence related to Ag NCs. Here, S_0 represent the ground state, S_1 is the excited singlet state, while T_1 and T_2 are the excited triplet states, respectively.[19]

When an excitation occurs with UV light, an electron undergoes a transition from the ground state S_0 to the excited singlet state S_1. As we can see from model involving the four-level, five possible emission transitions can occur around the blue, green, red, infrared and far infrared range of the spectrum originated from $S_1 \rightarrow S_0$, $T_2 \rightarrow S_0$, $T_1 \rightarrow S_0$, $S_1 \rightarrow T_1$ and $T_2 \rightarrow T_1$ transitions, respectively. First, the excitation at shorter-wavelength (between 270 and 330 nm) will transfer the electron to S_1 state giving rise to a blue.[19] On the other hand, an excitation wavelength near to 360 nm will excite the electron in a low-lying single state of S_1, which will rapidly relaxes to triplets excited states *via* slow triplet–singlet transitions $T_2 \rightarrow S_0$ (green-yellow emission) and $T_1 \rightarrow S_0$ (red emission),[19] in addition to the shorter singlet–singlet transition $S_1 \rightarrow S_0$ and then giving rise to a broad emission band almost covering the visible light region (from 400 to 800 nm). The last two transitions $S_1 \rightarrow T_1$ and $T_2 \rightarrow T_1$ are quenched non-radiatively by cross-relaxation energy transfer due to their relatively small energy/quantum resulting in increasing of yellow-red emission band $T_1 \rightarrow S_0$.[19]

In summary, three basic groups of Ag NCs are responsible for the blue, green and red luminescence. The blue emitting NCs have the smallest size, and the size of NCs increases from the blue to the green and further to the red with the increases of $AgNO_3$ concentration. This follows from the dependence of emission wavelength *versus* Ag doping level and also from direct structural measurements by transmission electron microscopy. The results of emission spectra dependence on Ag NCs concentrations indicates that the green and the red emissions bands becomes more prominent at the expense of the blue emission band which decrease with the increases of Ag doping level. Therefore, we conclude that when the "blue" Ag NCs reach a critical size, they apparently cease to emit and/or they transfer energy to "green" and "red" NCs.

Table 1 The measured lifetimes of 5 mol% $AgNO_3$ doped sample at different detected wavelengths

Emission at:	τ_{fast} (μs)	τ_{slow} (μs)
420 nm	11	68
550 nm	24	114
620 nm	39	131

IV. Conclusion

In this contribution, emission properties of silver NCs within fluorophosphate glassy matrices were studied. The findings show that the formation and the growth of NCs with different size are determined by glass-intrinsic reduction mechanisms. When excited under UV, Ag NCs dispersed in the glass matrix

exhibit single broad-band emission, covering the VIS range of the spectrum, giving rise to a white emission. It implies a broad range of applications such as light emitting diodes. Our present systematic study provides useful information for further development of nano-photonics devices.

Conflicts of interest

There are no conflicts to declare.

Acknowledgements

The authors acknowledge Brazilian agency FAPESP (grants numbers #2016/16343-2 and #2013/07793-6) for financial support.

References

1 I. Díez and R. H. A. Ras, *Nanoscale*, 2011, **3**, 1963–1970.
2 I. Díez, M. Pusa, S. Kulmala, H. Jiang, A. Walther, A. S. Goldmann, A. H. E. Müller, O. Ikkala and R. H. A. Ras, *Angew. Chem., Int. Ed.*, 2009, **48**, 2122–2125.
3 V. K. Tikhomirov, V. D. Rodríguez, A. Kuznetsov, D. Kirilenko, G. Van Tendeloo and V. V. Moshchalkov, *Opt. Express*, 2010, **18**, 22032–22040.
4 A. S. Kuznetsov, N. T. Cuong, V. K. Tikhomirov, M. Jivanescu, A. Stesmans, L. F. Chibotaru, J. J. Velázquez, V. D. Rodríguez, D. Kirilenko, G. Van Tendeloo and V. V. Moshchalkov, *Opt. Mater.*, 2012, **34**, 616–621.
5 V. D. Rodríguez, V. K. Tikhomirov, J. Mendez-Ramos, A. C. Yanes and V. V. Moshchalkov, *Sol. Energy Mater. Sol. Cells*, 2010, **94**(10), 1612–1617.
6 S. Roy, A. Baral and A. Banerjee, *ACS Appl. Mater. Interfaces*, 2014, **6**, 4050–4056.
7 S. Roy, A. Baral, R. Bhattacharjee, B. Jana, A. Datta, S. Ghosh and A. Banerjee, *Nanoscale*, 2015, **7**, 1912–1920.
8 A. Baral, K. Basu, S. Ghosh, K. Bhattacharyya, S. Roy, A. Datta and A. Banerjee, *Nanoscale*, 2017, **9**, 4419–4429.
9 S. Roy and A. Banerjee, *Soft Matter*, 2011, **7**, 5300–5308.
10 T. Udaya Bhaskara Rao and T. Pradeep, *Angew. Chem., Int. Ed.*, 2010, **49**, 3925–3929.
11 I. Díez and R. H. A. Ras, *Advanced Fluorescence Reporters in Chemistry and Biology II*, Springer, 2010, pp. 307–332.
12 G. T. Boyd, Z. H. Yu and Y. R. Shen, *Phys. Rev. B: Condens. Matter Mater. Phys.*, 1986, **33**, 7923–7936.
13 C. D. Geddes, A. Parfenov, I. Gryczynski and J. R. Lakowicz, *J. Phys. Chem. B*, 2003, **107**, 9989–9993.
14 I. Russier-Antoine, F. Bertorelle, R. Hamouda, D. Rayane, P. Dugourd, Ž. Sanader, V. Bonačić-Koutecký, P.-F. Breveta and R. Antoine, *Nanoscale*, 2016, **8**, 2892–2898.
15 A. S. Kuznetsov, V. K. Tikhomirov, M. V. Shestakov and V. V. Moshchalkov, *Nanoscale*, 2013, **5**, 10065–10075.
16 Z. Zhou, G. Liu, Q. Wei, H. Yang and Q. Liu, *J. Lumin.*, 2016, **169**, 695–700.
17 M. Yamane and Y. Asahara, *Glasses for Photonics*, Cambridge University Press, Cambridge, UK, 2000.
18 A. S. Kuznetsov, J. J. Velazquez, V. K. Tikhomirov, J. M. Ramos and V. V. Moshchalkov, *Appl. Phys. Lett.*, 2012, **101**, 251106–251110.
19 J. J. Velázquez, V. K. Tikhomirov, L. F. Chibotaru, N. T. Cuong, A. S. Kuznetsov, V. D. Rodrıguez, M. T. Nguyen and V. V. Moshchalkov, *Opt. Express*, 2012, **20**, 13582–13591.
20 N. T. Cuong, V. K. Tikhomirov, L. F. Chibotaru, A. Stesmans, V. D. Rodrıguez, M. T. Nguyen and V. V. Moshchalkov, *J. Chem. Phys.*, 2012, **136**, 174108–174116.
21 K. H. Park, S. H. Im and O. O. Park, *Nanotechnology*, 2011, **22**, 045602–045607.
22 G. Galleani, S. H. Santagneli, Y. Messaddeq, M. de Oliveira Jr and H. Eckert, *Phys. Chem. Chem. Phys.*, 2017, **19**, 21612–21624.
23 V. A. Aseev, P. A. Burdaev, E. V. Kolobkova and N. V. Nikonorov, *Glass Phys. Chem.*, 2012, **38**, 366–372.
24 V. K. Tikhomirov, D. Furniss, I. M. Reaney, M. Beggiora, M. Ferrari, M. Montagna and R. Rolli, *Appl. Phys. Lett.*, 2002, **81**, 1937–1939.
25 M. Eichelbaum and K. Rademann, *Adv. Funct. Mater.*, 2009, **19**, 2045–2052.
26 K. Baishya, J. C. Idrobo, S. Öğüt, M. Yang, K. Jackson and J. Jellinek, *Phys. Rev. B: Condens. Matter Mater. Phys.*, 2008, **78**, 075439–075447.
27 M. Pereiro and D. Baldomir, *Phys. Rev. A*, 2007, **75**, 033202–033211.
28 J. Zheng, P. R. Nicovich and R. M. Dickson, *Annu. Rev. Phys. Chem.*, 2007, **58**, 409–431.
29 X. Y. Liu, H. Guo, S. Ye, M. Y. Peng and Q. Y. Zhang, *J. Mater. Chem. C*, 2015, **3**, 5183–5191.
30 A. Kulesza, R. Mitric, V. Bonacic-Koutecky, B. Bellina, I. Compagnon, M. Broyer, R. Antoine and P. Dugourd, *Angew. Chem., Int. Ed.*, 2011, **50**, 878–881.
31 H. Lin, D. Chen, Y. Yu, R. Zhang and Y. Wang, *Appl. Phys. Lett.*, 2013, **103**, 091902–091905.
32 E. Borsella, F. Gonella, P. Mazzoldi, A. Quaranta, G. Battaglin and R. Polloni, *Chem. Phys. Lett.*, 1998, **284**, 429–434.
33 A. S. Kuznetsov, V. K. Tikhomirov and V. V. Moshchalkov, *Mater. Lett.*, 2013, **92**, 4–6.
34 M. V. Shestakov, X. Chen, W. Baekelant, A. S. Kuznetsov, V. K. Tikhomirov, J. Hofkens and V. V. Moshchalkov, *RSC Adv.*, 2014, **4**, 20699–20703.
35 H. Xu and K. Suslick, *ACS Nano*, 2010, **4**, 3209–3214.
36 S. Choi, R. M. Dickson and J. Yu, *Chem. Soc. Rev.*, 2012, **41**, 1867–1891.
37 W. Chen, A. G. Joly and J. Roark, *Phys. Rev. B: Condens. Matter Mater. Phys.*, 2002, **65**, 245404.
38 M. V. Shestakov, N. T. Cuong, V. K. Tikhomirov, M. T. Nguyen, L. F. Chibotaru and V. V. Moshchalkov, *J. Phys. Chem. C*, 2013, **117**, 7796–7800.